Fig. S1

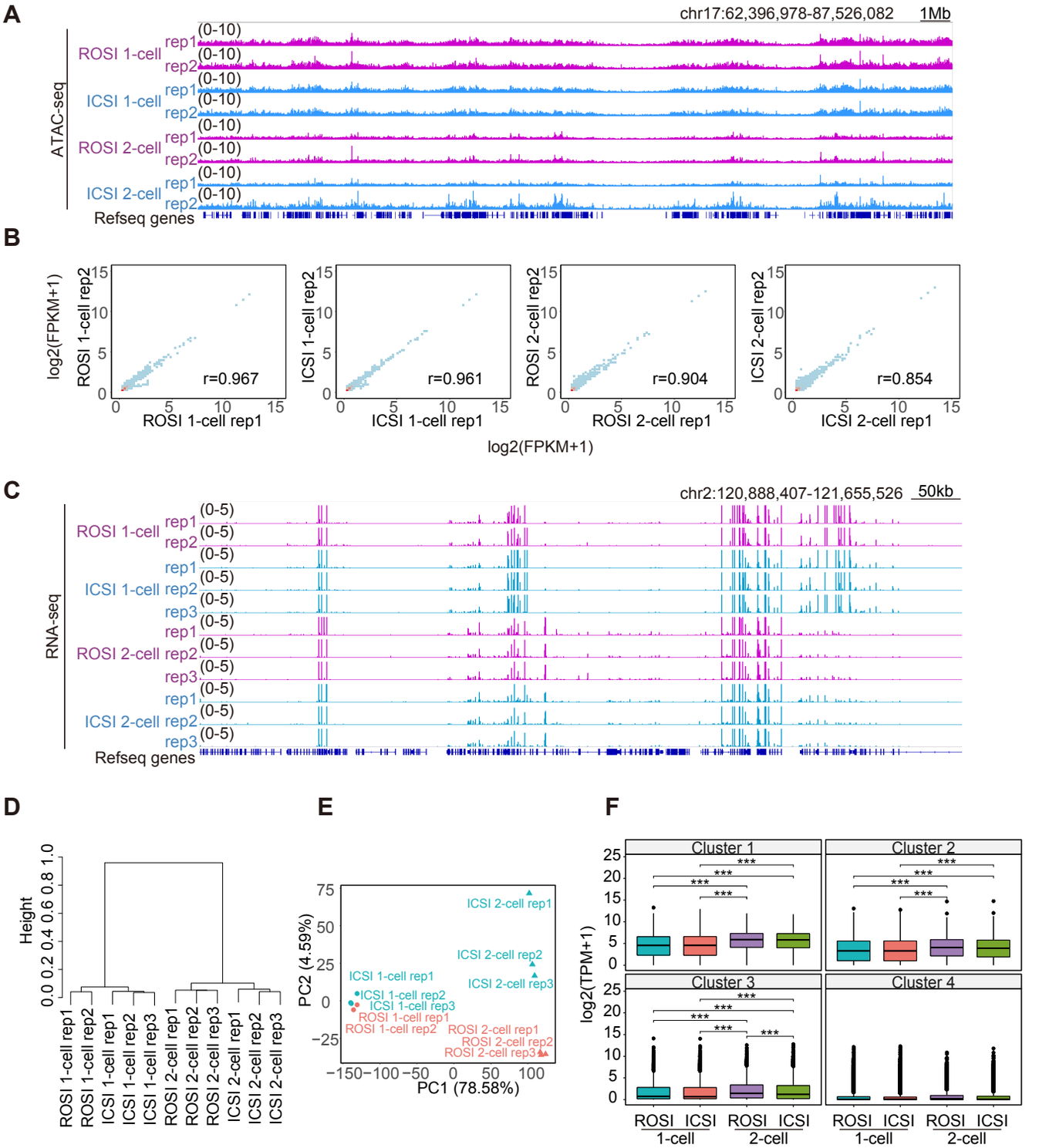

Fig. S1. Validation of ATAC-seq and RNA-seq among replications.
(A) Genome browser snapshots showing ATAC-seq replications. ATAC-seq data are shown as RPKM.
(B) Scatter plots showing ATAC-seq replications. ATAC-seq enrichment was calculated as FPKM (10 kb window for the entire genome). Pearson correlation coefficients are shown.
(C) Genome browser snapshots among RNA-seq replications.
(D) Hierarchical clustering of the global gene expression pattern among RNA-seq replications.
(E) Principal component analysis (PCA) of global gene expression pattern among RNA-seq replications. Red and blue show ROSI and ICSI-embryos, respectively. Circle and triangle symbols show the 1-cell and 2-cell stages, respectively. PCA was calculated log2 (1+TPM) value. The variance of PC1 is 78.58% and PC2 is 4.59%.
(F) Box plots showing expression kinetics among cluster defined by k-means cluster from ATAC-seq TSS signal. ***p < 0.001 and FDR < 0.05, Tukey-Kramer method.

Fig. S2

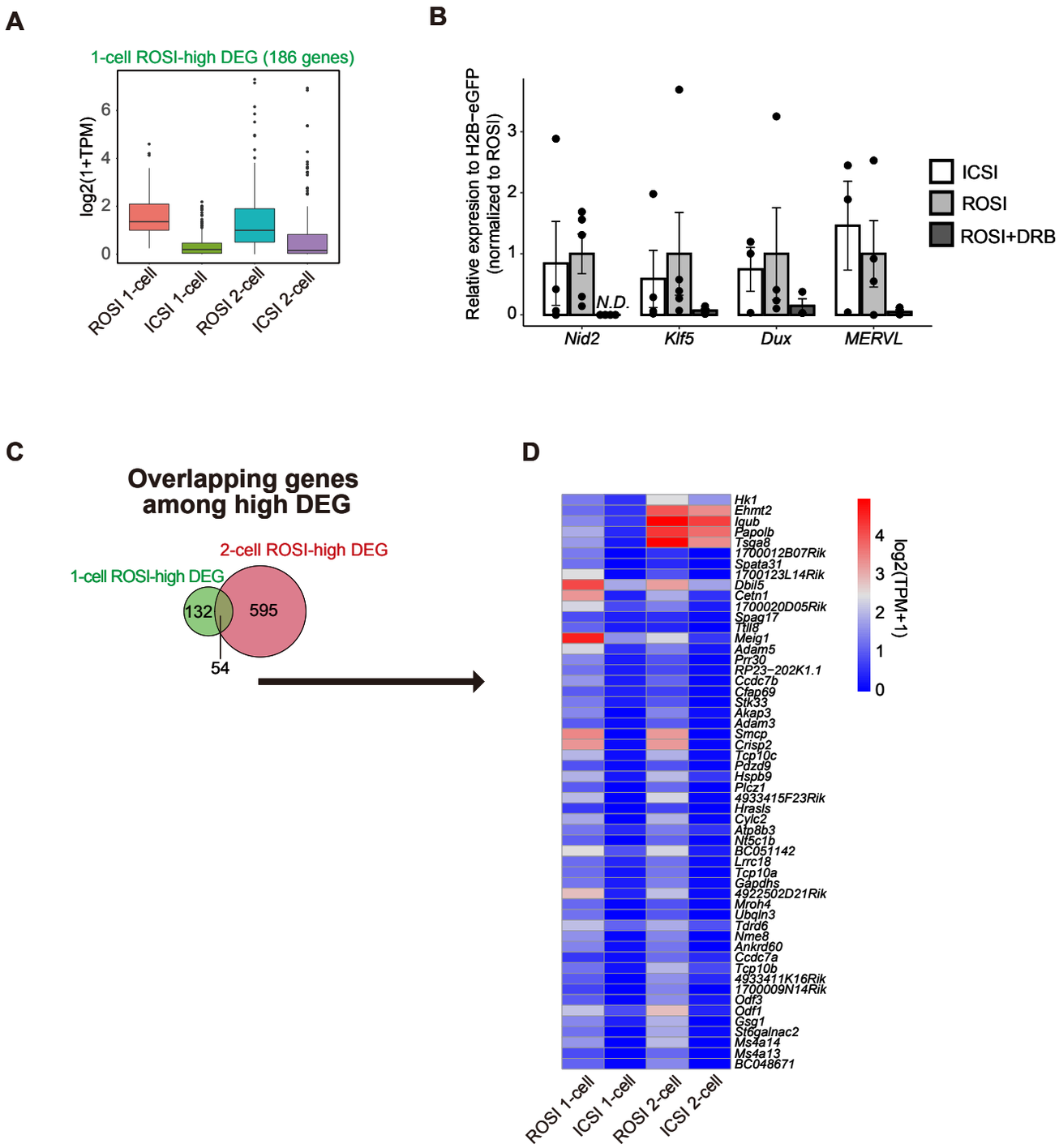

Fig. S2. Features of differentially expressed genes (DEGs) in ROSI-embryos.

(A) Box plots showing expression kinetics of 1-cell ROSI-high DEGs.

(B) DRB (5,6-dichloro-1-β-D-ribofuranosyl-benzimidazole) inhibits transcription as reported by Abe et al., 2018. Quantitative real-time PCR analyses of minor ZGA genes (*Nid2*, *Klf5*, *Dux*, and *MERVL*) and H2B-eGFP as an external control expression in 1-cell ICSI, ROSI, and DRB-treated ROSI-embryos (at least three biological replicates). Gene expression was first normal-ized using the expression of H2B-eGFP and divided by the mean value of ROSI-embryos. Data are presented as the mean value. Error bars indicate the standard error of the mean. Dots indicate each data point. *Nid2* was not detected in DRB-treat-ed ROSI-embryos.

(C) Overlapping genes between 1-cell ROSI-high-DEG and 2-cell ROSI-high DEG. A total of 54 genes overlapped.

(D) Heatmap showing expression kinetics of overlapped genes of ROSI-high DEG as shown in (C).

Fig. S3

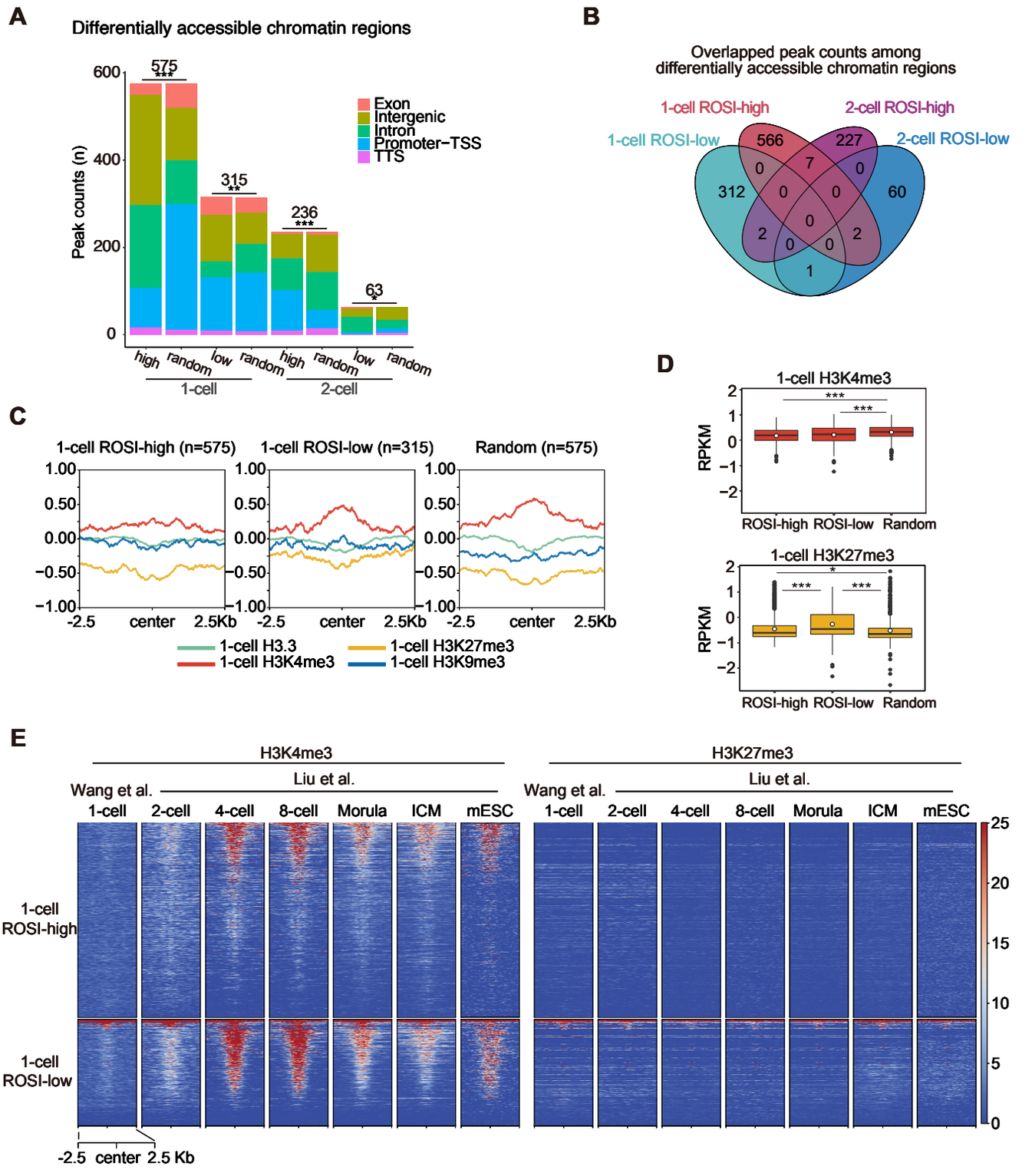

Fig. S3. Features of differentially accessible chromatin regions.
(A) The genomic location of each peak and randomly selected peaks from all the peaks of ROSI 1-cell or 2-cell all peaks. Asterisks indicate significant differences as *p<0.05, **p<0.01, and *** p< 0.001 (Fisher's Exact Test).
(B) Venn diagrams showing the overlap between each group of differentially accessible chromatin regions.
(C) Enrichment of histone modifications and H3.3 at the 1-cell stage around the regions of differentially accessible chromatin regions and randomly selected regions from all the ATAC peaks of ROSI 1-cell. ChIP-seq data for H3.3, H3K4me3, H3K27me3, and H3K9me3 at the 1-cell stage are from GSE139527 and GSE97778 (Ishiuchi et al., 2021; Wang et al., 2018). ChIP-seq data are shown as RPKM for log2 ratios between ChIP and input samples.
(D) Enrichments of H3K4me3 (upper) and H3K27me3 (lower) are represented as box plots. Open circles indicate mean values. Asterisks indicate significant differences as *p<0.05, **p<0.01, and *** p< 0.001 (Tukey-Kramer test).
(E) Heatmaps showing normalized H3K4me3 (left) and H3K27me3 (right) in each stage of pre-implantation embryos and mouse ES cells (mESC) around 1-cell ROSI-high and ROSI-low ATAC peaks. ChIP-seq data for H3K4me3 and H3K27me3 are from GSE97778 and GSE73952 (Liu et al., 2016; Wang et al., 2018). ChIP-seq enrichment is shown as RPKM values.

Fig. S4

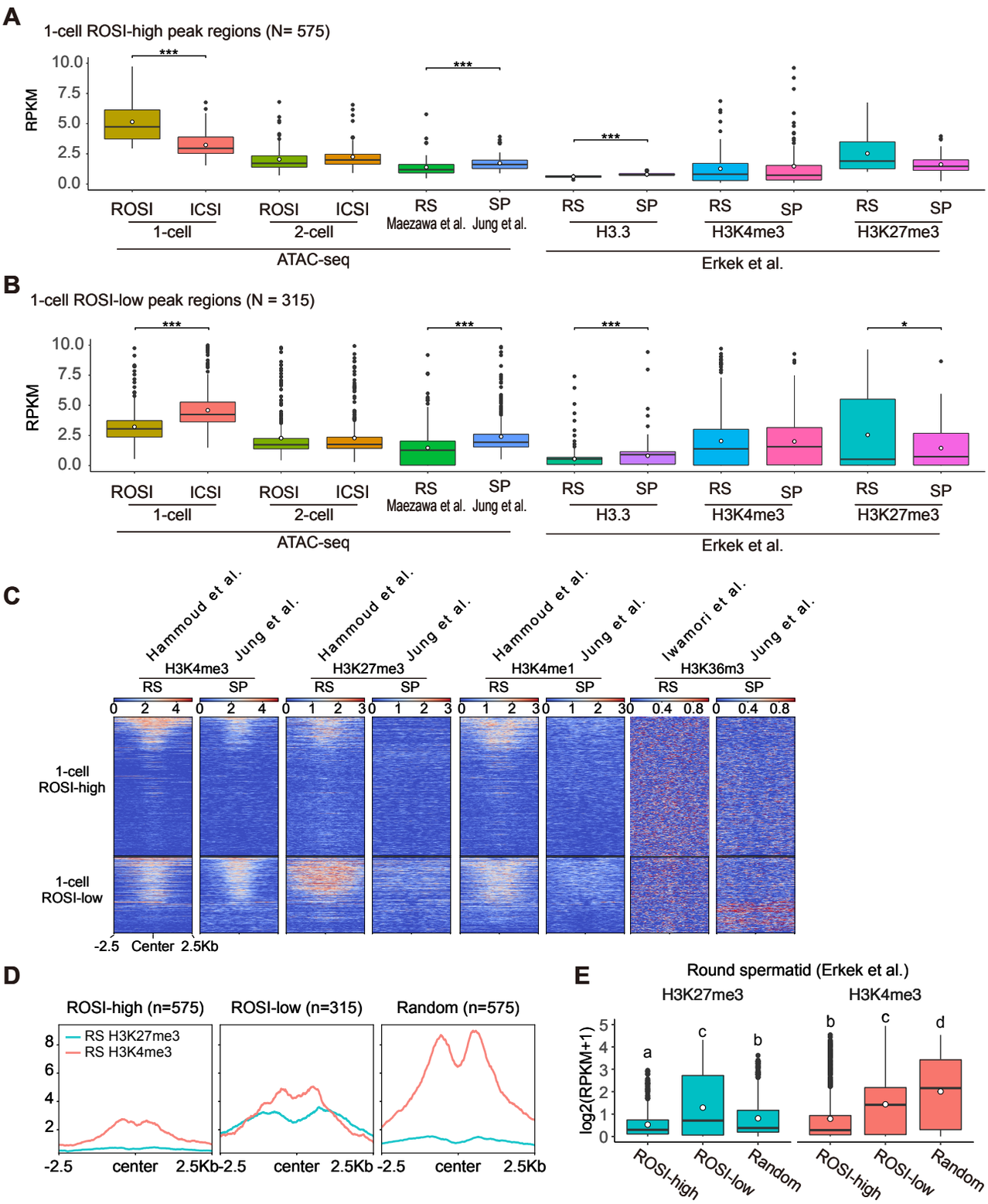

Fig. S4. Characterization of differentially accessible chromatin regions in round spermatids and sperm.

(A and B) Box plots showing ATAC-seq data and ChIP-seq data for H3.3, H3K4me3, and H3K27me3 in differentially accessi-ble chromatin regions. ATAC-seq and ChIP-seq data for round spermatid (RS) and sperm (SP) were obtained from GSE102954, GSE116857, and GSE42629 (Erkek et al., 2013; Jung et al., 2019; Maezawa et al., 2018a). Box plots shown with RPKM in each peak center ± 2,5kb, and open circles are presented as mean values. Asterisks indicate significant differences as *p<0.05, **p<0.01, and *** p< 0.001 (Wilcoxon Rank Sum test). Box plots showing the 1-cell ROSI-high peak regions (A), and 1-cell ROSI-low peak regions (B).

(C) Heatmaps showing ChIP-seq data for H3K4me3, H3K27me3, H3K4me1, and H3K36me3 in differentially accessible chromatin regions. ChIP-seq data for round spermatid (RS) and sperm (SP) were obtained from GSE49624, GSE79230, and DRA004778 (Hammoud et al., 2014; Jung et al., 2017; Iwamori et al., 2016). Heatmaps are shown with RPKM for log2 ratios between ChIP and input samples (H3K4me3, H3K27me3, H3K4me1, and H3K36me3).

(D and E) Enrichment of H3K27me3 and H3K4me3 in round spermatids (Erkek et al., 2013) of differentially accessible chromatin regions and randomly selected regions from ROSI 1-cell all ATAC peaks. (D) The enrichment was shown as the average value around the peak center of each region. (E) The enrichment was represented as box plots. Open circles indicate mean values. Different characters indicate significant differences (Tukey–Kramer test).

Fig. S5

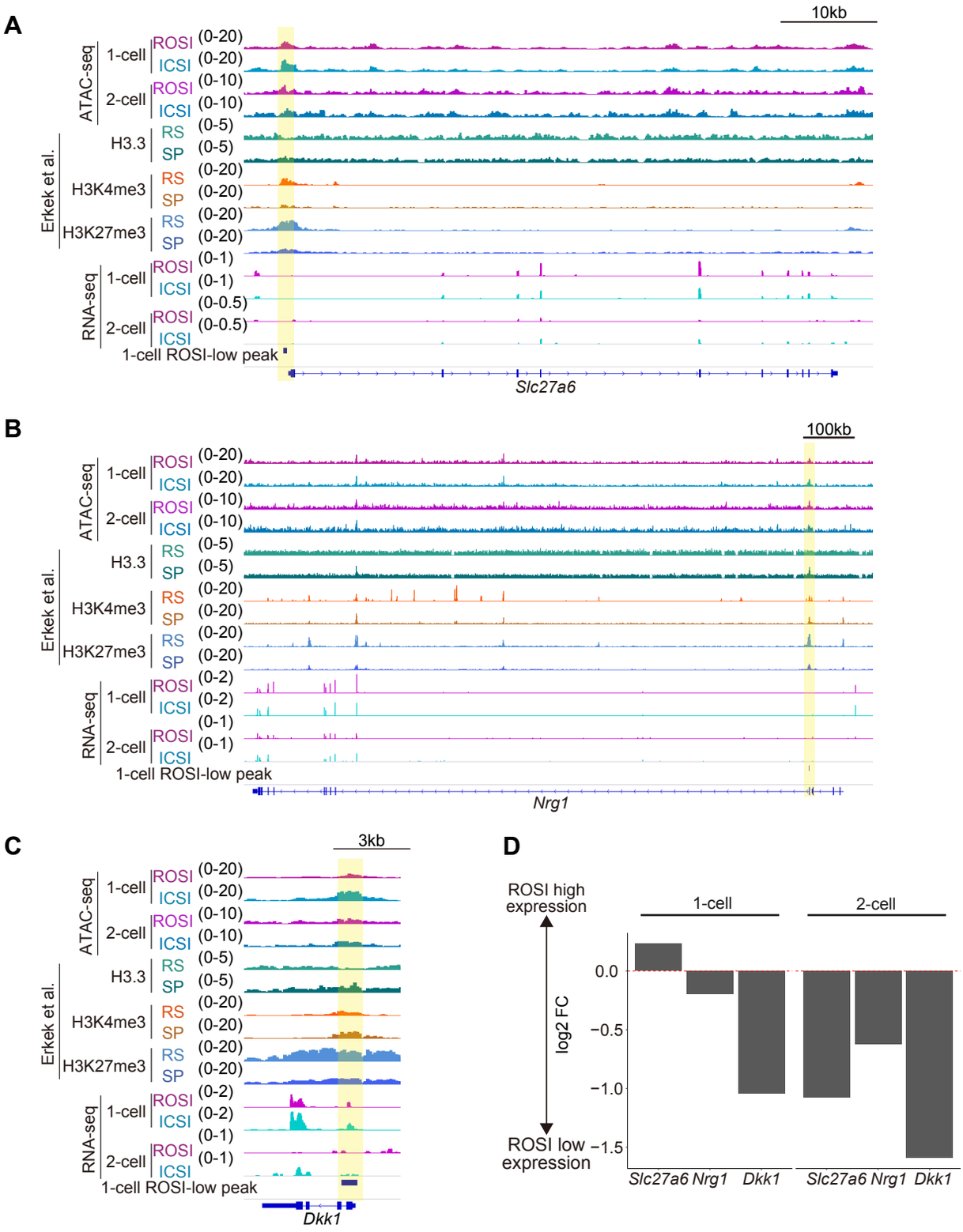

Fig. S5. Genome browser snapshots and gene expression of 1-cell ROSI-low ATAC peak regions.
(A, B, and C) Genome browser snapshots showing representative genes (*Slc27a6* (A), *Nrg1*(B), and *Dkk1*(C)) with decreased promoter chromatin accessibility in 1-cell ROSI-embryos. The 1-cell ROSI-low peak regions are highlighted in light yellow. ChIP-seq data for round spermatid (RS) and sperm (SP) were obtained from GSE42629 (Erkek et al., 2013).
(D) Bar plots showing differences in representative genes between ROSI- and ICSI-embryos at the 1-cell and 2-cell stages.

Fig. S6

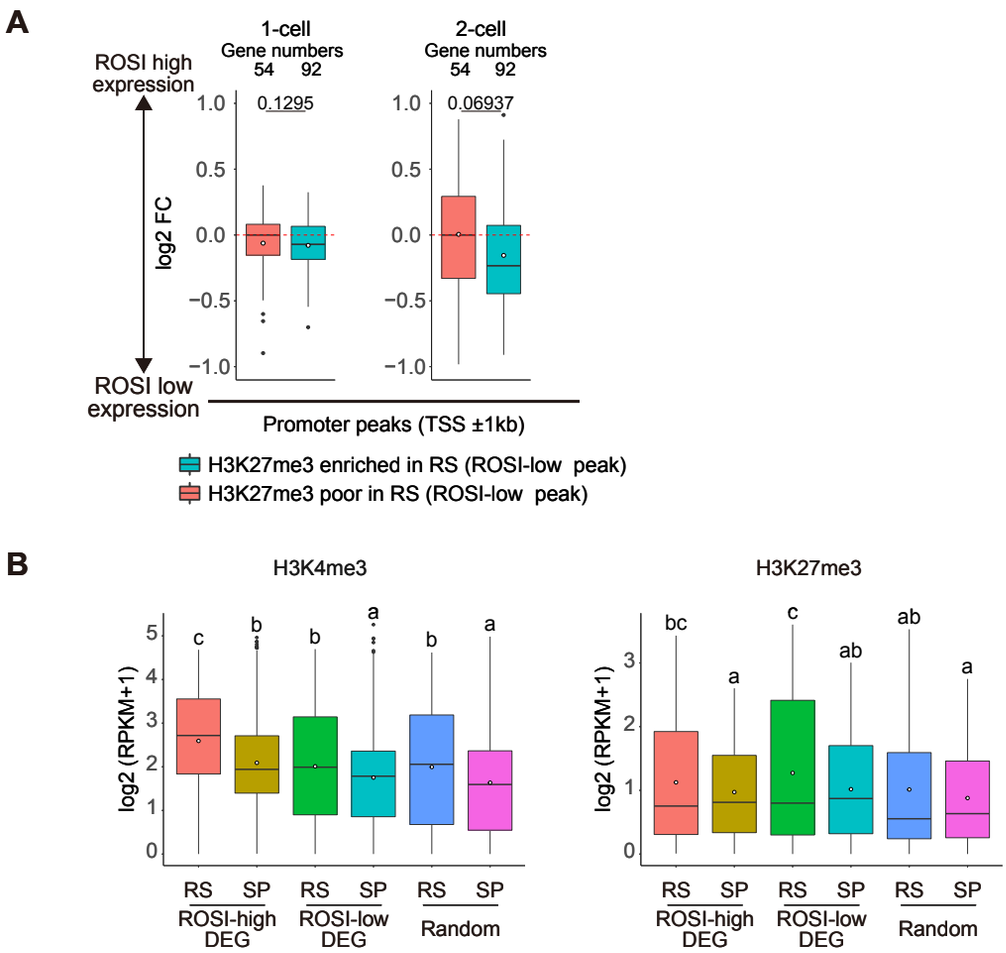

Fig. S6. Altered gene expression in the region with HK27me3 enrichment in round spermatids. (A) Box plots showing differences in gene expression between ROSI- and ICSI-embryos at the 1- or the 2-cell stages. ATAC promoter peak regions (TSS ± 1kb) within ROSI-low peak regions were divided into two groups “H3K27me3 enriched in RS” (blue) and “H3K27me3 poor in RS” (red) peaks. Then, the expression was analyzed on the genes associ-ated with these ATAC peak regions. Open circles represent the mean values. The number of genes in each group is indicated above the box plots. The p values were calculated using Wilcoxon rank-sum test.
(B) Box plots showing the enrichment of H3K4me3 (left) and H3K27me3 (right) in round spermatid (RS) or sperm (SP) of each DEG group and randomly selected genes as RPKM values. Open circles represent the mean values. Different characters indicate significant differences (Tukey-Kramer test).

Fig. S7

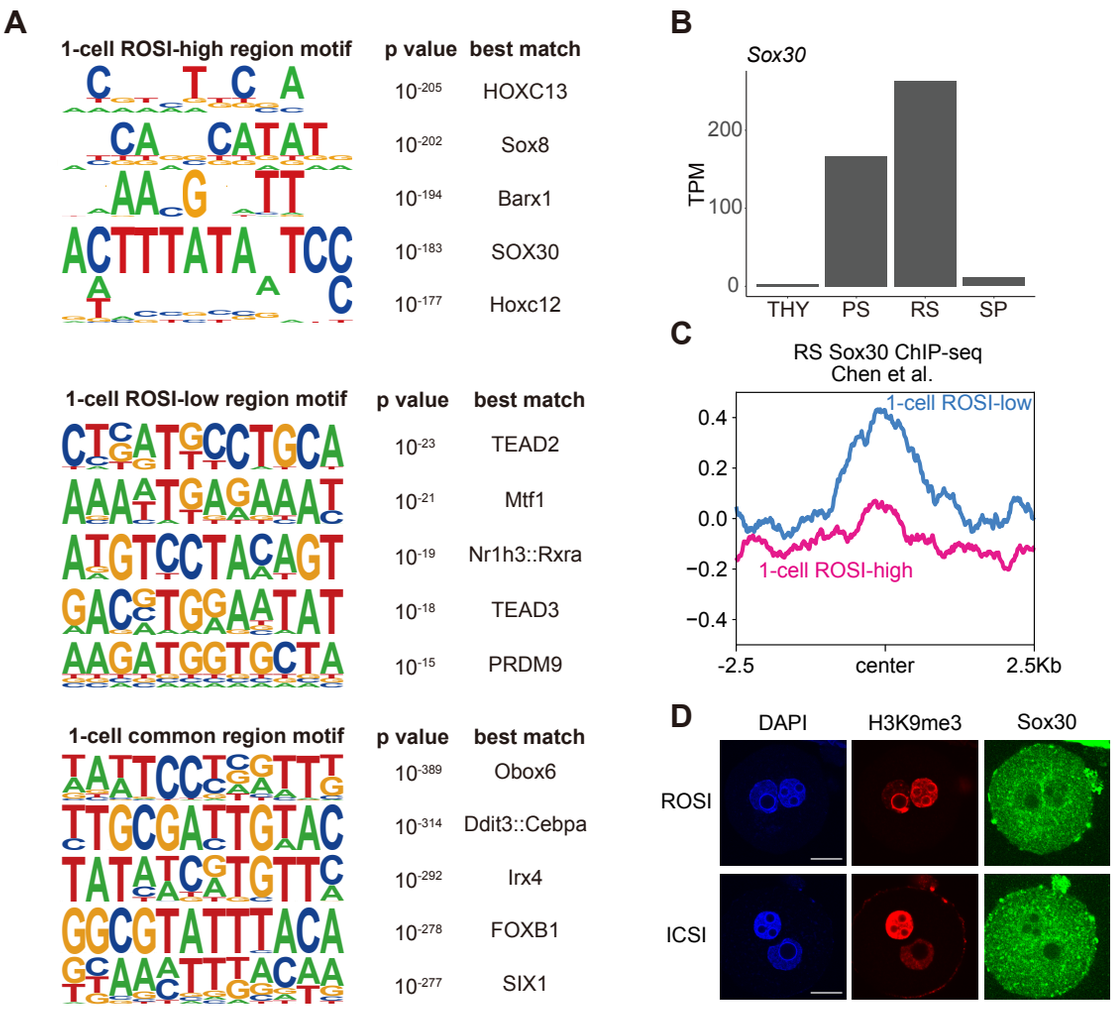

Fig. S7. Motif analysis of 1-cell ROSI high peak regions

(A) Motif analysis of ATAC-peak classified 1-cell ROSI as high, low and common peak for putative transcription factor (TF) binding site was performed using HOMER (Heinz et al., 2010) and the top of five motifs were shown.

(B) Expression value of *Sox30* during representative stages of spermatogenesis; THY undifferentiated spermatogonia; PS pachytene spermatocytes; RS round spermatid; SP sperm. Published RNA-seq data (GSE55060 and DRA000484)

(Hasegawa et al., 2015; Kobayashi et al., 2012) were used.

(C) The enrichment of SOX30 in round spermatids using published ChIP-seq data (GSE107644) (Chen et al., 2018b). SOX30 enrichment is shown as RPKM for log2 ratios among input data and colored with pink and blue around 1-cell ROSI-high peak regions and ROSI-low peak regions, respectively.

(D) Images of immunostaining for Sox30 and H3K9me3 in ROSI- and ICSI-embryos at the 1-cell stage. Scale bar, 20 μm.

Table S1. Differential chromatin accessible regions and gene expression

Click here to download Table S1